

Absorption Spectra and Photochemical Reactions in a Unique Photoactive Protein, Middle Rhodopsin MR

Keiichi Inoue,^{†,‡} Louisa Reissig,^{‡,§} Makoto Sakai,[§] Shiori Kobayashi,[‡] Michio Homma,[‡] Masaaki Fujii,[§] Hideki Kandori,[†] and Yuki Sudo^{*,‡,||}

[†]Department of Frontier Materials, Nagoya Institute of Technology, Showa-ku, Nagoya, 466-8555, Japan

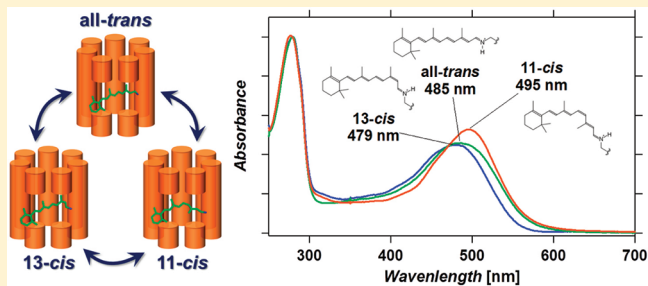
[‡]Division of Biological Science, Graduate School of Science, Nagoya University, Nagoya, 464-8602, Japan

[§]Chemical Resources Laboratory, Tokyo Institute of Technology, 4259 Nagatsuta-cho, Midori-ku, Yokohama 226-8503, Japan

^{||}PRESTO, Japan Science and Technology Agency (JST), 4-1-8 Honcho Kawaguchi, Saitama, 332-0012, Japan

S Supporting Information

ABSTRACT: Photoactive proteins with cognate chromophores are widespread in organisms, and function as light-energy converters or receptors for light-signal transduction. Rhodopsins, which have retinal (vitamin A aldehyde) as their chromophore within their seven transmembrane α -helices, are classified into two groups, microbial (type-1) and animal (type-2) rhodopsins. In general, light absorption by type-1 or type-2 rhodopsins triggers a *trans*-*cis* or *cis*-*trans* isomerization of the retinal, respectively, initiating their photochemical reactions. Recently, we found a new microbial rhodopsin (middle rhodopsin, MR), binding three types of retinal isomers in its original state: all-*trans*, 13-*cis*, and 11-*cis*. Here, we identified the absolute absorption spectra of MR by a combination of high performance liquid chromatography (HPLC) and UV-vis spectroscopy under varying light conditions. The absorption maxima of MR with all-*trans*, 13-*cis*, or 11-*cis* retinal are located at 485, 479, and 495 nm, respectively. Their photocycles were analyzed by time-resolved laser spectroscopy using various laser wavelengths. In conclusion, we propose that the photocycles of MR are $MR(trans) \rightarrow MR_K: \text{lifetime} = 93 \mu\text{s} \rightarrow MR_M: \text{lifetime} = 12 \text{ ms} \rightarrow MR$, $MR(13-cis) \rightarrow MR_{O-like}: \text{lifetime} = 5.1 \text{ ms} \rightarrow MR$, and $MR(11-cis) \rightarrow MR_{K-like}: \text{lifetime} = 8.2 \mu\text{s} \rightarrow MR$, respectively. Thus, we demonstrate that a single photoactive protein drives three independent photochemical reactions.



INTRODUCTION

Rhodopsins are membrane-embedded photoreceptor proteins, which have seven transmembrane α -helices and retinal as a chromophore (vitamin A aldehyde). They are, in general, classified into two groups, microbial (type-1) and animal (type-2) rhodopsins.¹ In the past years, over 4000 examples of type-1 rhodopsins have been isolated from organisms widespread in the microbial world, including prokaryotes (bacteria and archaea) and eukaryotes (fungi and algae).² Also, many examples of type-2 rhodopsins, which include, for example, visual pigments belonging to the G-protein coupled receptor (GPCR) family, have been reported in vertebrates and invertebrates.³ Despite the structural similarities of these proteins, their physiological functions can differ significantly. For example, a number of type-1 rhodopsins have been reported to be light-driven ion pumps, such as bacteriorhodopsin (BR) in haloarchaea, xanthorhodopsin in halophilic bacteria, proteorhodopsin in marine bacteria, *Leptosphaeria* rhodopsin in fungi,^{2,4,5} and halorhodopsin (HR) in haloarchaea and eubacteria. In addition, a light-gated cation channel, channel rhodopsin (ChR), has been found in *Chlamydomonas*.^{6,7} On the other hand, some isolated microbial rhodopsins have, instead,

shown a signal transduction function upon the binding of their respective transducers. For example, sensory rhodopsin I (SRI) and II (SRII), which have been found in haloarchaea and eubacteria, transmit a signal to change the rotation pattern of the flagellar motor, resulting in a positive taxis of the cells toward green-orange light and a negative taxis from blue and near-UV light.⁸ Furthermore, it has been predicted that *Anabaena* sensory rhodopsin (ASR) functions as a photosensor protein of the gene expression in response to the color and intensity of light.⁹ In general, the functions of type-1 rhodopsins can be, to a large extent, divided into light-driven ion transporters and signaling light-sensors, while many type-2 rhodopsins found so far are coupled to a G-protein, and mediate a GDP–GTP exchange reaction.^{3,10}

The biological functions of rhodopsin molecules are triggered by light absorption. Many type-1 rhodopsins have all-*trans* retinal in the original state, and this retinal chromophore is isomerized to 13-*cis* by photoactivation.

Received: March 12, 2012

Revised: April 25, 2012

Published: April 30, 2012

However, there exist also those, like BR or ASR, which accommodate both all-*trans* and 13-*cis* retinal in the original state, which can be interconverted by illumination.¹¹ In contrast, many type-2 rhodopsins have 11-*cis* retinal in the original state, which is isomerized to all-*trans* by photoactivation. Recently, we found a new type-1 rhodopsin molecule from *Haloquadratum walsbyi* (named middle rhodopsin, MR), possessing characteristic properties of both BR and SRII.¹² Interestingly, MR shows a broad absorption spectrum with the absorption maximum located at 485 nm. In addition to this, high performance liquid chromatography (HPLC) analysis indicated that MR has the unique character of binding a mixture of all-*trans*, 13-*cis*, and 11-*cis* retinal isomers in the dark (Figure 1).¹² It should be noted that this was the

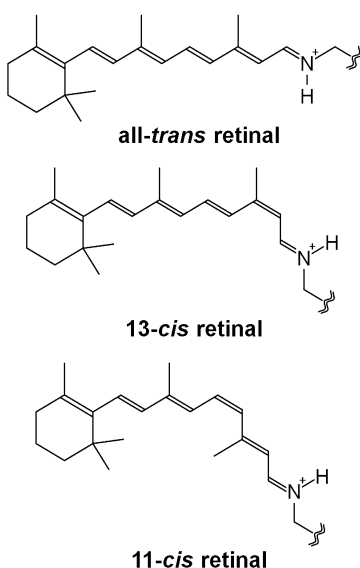


Figure 1. Chemical structures of three types of retinal isomers: all-*trans*, 13-*cis*, and 11-*cis*.

first finding of a microbial rhodopsin which binds 11-*cis* retinal, a feature commonly found only among type-2 rhodopsins.¹³ Although the configurations of C15=N of those MR isomers have not been determined yet, the 15-syn form can be expected, similar to other type-1 rhodopsins, including 13-*cis* BR. The 13-*cis*-15-*anti* or 11-*cis*-15-*anti* configurations have a drastically different shape compared with all-*trans* retinal, and would, therefore, impose a strong distortion on the peptide backbone which is likely to result in the destabilization of the protein. The retinal composition has been reported to be changed from a ratio of, e.g., all-*trans*:13-*cis*:11-*cis* = 36.5%:56.4%:7.6% in a dark adapted state to 17.8%:47.7%:30.1% after light adaptation for a specific wavelength. On the basis of this complexity in retinal composition and dark-light adaptation, it has been suggested that the photocycle of MR is significantly different from previously investigated type-1 and type-2 rhodopsins.

In this study, the photoreaction dynamics of MR were investigated by laser flash photolysis. As the transient spectral changes, representing photoreaction of each isomer, overlap with each other, the signals were experimentally decomposed in order to determine which observed reaction components originated from which isomer. This was achieved by using multicolor spectroscopy with various excitation wavelengths. For the exact interpretation of the spectral changes, the relative

abundance of each retinal isomer in the light adapted state was obtained by a combination of HPLC and UV-vis analysis. From these results, the absolute absorption spectra of each isomer of MR could be extracted mathematically. These absolute absorption spectra were compared to the observed relative intensities of each component in the transient absorption change depending on excitation wavelength. By doing so, and by making use of the knowledge about rhodopsin photocycles based on previous studies, the respective photocycles of all MR isomers could be determined. The obtained results give new insight into the regulation of the photoisomerization in the protein moiety.

MATERIALS AND METHODS

Sample Preparations. The expression plasmid of MR was constructed by the method described previously.¹² Cells with the plasmid were grown in LB medium, supplemented with ampicillin (final concentration of 50 µg/mL). *E. coli* BL21-(DE3) cells, harboring the plasmid, were grown to an OD₆₆₀ of 0.3–0.5 in a 30 °C incubator, followed by the addition of 0.5 mM isopropyl-β-D-1-thiogalactopyranoside (IPTG).¹² Cells were harvested 10 h postinduction at 18 °C by centrifugation at 4 °C, and were then resuspended in buffer S (50 mM 2-(N-morpholino)ethanesulfonic acid (MES), 1 M NaCl, pH 6.5), and disrupted by sonication, or by using a French press. Cell debris was removed by low speed centrifugation (5000g, 10 min, 4 °C). Crude membranes were then collected by high speed centrifugation (100 000g, 30 min, 4 °C), and washed with buffer S. For the solubilization of the membranes, 2% (w/v) *n*-dodecyl-β-D-maltoside (DDM) was added, and the suspension was incubated for 30 min at 4 °C. The solubilized membranes were isolated by high speed centrifugation (100 000g, 30 min, 4 °C), and the supernatant was applied to a Ni-affinity column (HisTrap, GE Healthcare, Uppsala, Sweden) at 4 °C in the dark. Thereafter, the column was extensively washed with buffer W (50 mM MES, 1 M NaCl, 20 mM imidazole, 0.05% DDM, pH 6.5) to remove unspecifically bound proteins. The histidine-tagged proteins were then eluted using a linear gradient of up to 100% elution buffer E (50 mM tris(hydroxymethylaminomethane (Tris-Cl), 1 M NaCl, 500 mM imidazole, 0.05% DDM, pH 7.0). The eluted proteins were then further applied to a HiTrapQ ion-exchange column (GE Healthcare) at 4 °C in buffer L (50 mM Tris-Cl, 30 mM NaCl, 0.05% DDM, pH 7.5). Thereafter, the column was extensively washed with buffer L to remove unspecifically bound proteins. The proteins were then eluted using a linear gradient of up to 100% elution buffer H (50 mM Tris-Cl, 1 M NaCl, 0.05% DDM, pH 7.5). The eluted proteins were further purified by a Sephadryl S-400 HR gel-filtration column (Amersham Biosciences, Pittsburgh, PA, USA) in buffer I (50 mM Tris-Cl, 1 M NaCl, 0.05% DDM, pH 7.0). The sample was concentrated for storage. Before each measurement, the sample was resuspended in buffer I.

HPLC and UV-vis Measurements. High performance liquid chromatography (HPLC) analysis, combined with UV-visible spectroscopy (UV2450 spectrophotometer, Shimadzu, Japan, λ = 250–800 nm), was used to study the retinal composition and optical properties of eight MR samples in the dark and after illumination with light of a specific range of wavelengths. The stability of the samples and their retinal compositions could be confirmed over a period of at least 2 h. Each sample was dark adapted for several days, after which the absorption spectra and the composition were determined. The

Table 1. Illumination Wavelengths λ_{ill} and Normalized All-trans, 13-cis, and 11-cis Retinal Compositions of the Analyzed MR Samples (1–8 from the Top)^a

λ_{ill} (nm)	all-trans			13-cis			11-cis		
	dark	light	dif.	dark	light	dif.	dark	light	dif.
450	47.309	27.317	-19.992	46.849	33.823	-13.026	5.842	38.860	+33.018
480	45.179	24.048	-21.131	49.980	37.970	-12.010	4.841	37.982	+33.141
500	43.118	22.785	-20.333	52.398	40.745	-11.653	4.484	36.470	+31.986
520	44.041	22.379	-21.662	51.483	42.727	-8.756	4.476	34.894	+30.418
550	44.079	19.948	-24.131	48.920	45.962	-2.958	7.001	34.090	+27.089
570	43.829	21.965	-21.864	51.602	48.604	-2.998	4.569	29.431	+24.862
600	42.460	32.360	-10.100	52.980	59.520	+6.540	4.560	8.120	+3.560
640	44.424	44.218	-0.206	51.345	51.571	+0.226	4.231	4.211	-0.020

^aThe compositions were obtained by HPLC analysis after adaptation in the dark for several days, and after 20 min of illumination with light of λ_{ill} . All compositions were normalized to obtain $c_{\text{AT}} + c_{13\text{cis}} + c_{11\text{cis}} = 100\%$. The difference composition Δc was calculated by subtracting the dark adapted composition from the light adapted composition. The accuracy of the illumination wavelengths is about 2%.

small variation in the retinal conformation between all the dark adapted samples supports the sufficient equilibration time of the samples. These samples were then illuminated with light of a particular wavelength λ_{ill} (see Table 1), and again analyzed. Because of trace amounts of other retinal conformations, such as 9-cis, which were not considered in this study, the compositions of all-trans, 13-cis, and 11-cis retinal have been normalized for comparison, leading to comparably small changes in numbers. The UV-vis spectra were normalized according to the peak around 280 nm originating from Tyr and Trp residues in the protein moiety. For the light activation, a 300 W Xe light source (Max-302, Asahi spectra, Japan) was employed with several kinds of band-pass filters (center wavelength \pm half-bandwidth: 450 ± 10 , 480 ± 10 , 500 ± 10 , 520 ± 10 , 550 ± 10 , 570 ± 10 , 600 ± 12 , and 640 ± 12 nm, Asahi spectra, Japan).

Extraction of the Single Component UV-vis Spectra.

Due to the comparable simplicity of the required multi-component analysis of the obtained data which have a high signal-to-noise ratio, compared to problems arising from, e.g., time-resolved spectroscopy (for more information on advanced mathematical methods, see, e.g., refs 14 and 15), the following mathematical analysis could be used to extract the single component UV-vis spectra of proteins binding all-trans, 11-cis, and 13-cis retinal from the experimentally combined UV-vis spectra (see Figure 2): each spectrum S_i of sample i was assumed to represent a linear combination of the spectra S_{AT} , $S_{13\text{cis}}$, and $S_{11\text{cis}}$, corresponding to the single component spectra of MR having all-trans, 13-cis, and 11-cis retinal, respectively, with coefficients corresponding to the retinal composition c_i in the sample which were obtained by HPLC analysis:

$$S_i = c_{\text{AT},i} S_{\text{AT}} + c_{13\text{cis},i} S_{13\text{cis}} + c_{11\text{cis},i} S_{11\text{cis}} \quad (1)$$

The difference spectra ΔS_i were calculated by subtracting the spectrum obtained in the dark adapted state from that in the light adapted state (Figure 2a and b). The changes in the sample illuminated with light of $\lambda_{\text{ill}} = 640$ nm were comparably small, and therefore, this difference spectrum was not used in the further analysis. For the difference spectrum ΔS_i , an equation, equivalent to eq 1, can be written, using the calculated changes in retinal composition Δc_i as coefficients:

$$\Delta S_i = \Delta c_{\text{AT},i} S_{\text{AT}} + \Delta c_{13\text{cis},i} S_{13\text{cis}} + \Delta c_{11\text{cis},i} S_{11\text{cis}} \quad (2)$$

By subtracting two difference spectra ΔS_n and ΔS_m multiplied by coefficients a_{nm} and b_{nm} , from the spectrum S_i , the single

component spectra $S_{x,nm}$ ($S_{\text{AT},nm}$, $S_{13\text{cis},nm}$, or $S_{11\text{cis},nm}$) can be isolated (Figure 2c–e)

$$S_{x,nm} = S_i - a_{nm}\Delta S_n - b_{nm}\Delta S_m \quad (3)$$

where a_{nm} and b_{nm} solve

For $S_{\text{AT},nm}$:

$$c_{11\text{cis},i} - a_{nm}\Delta c_{11\text{cis},n} - b_{nm}\Delta c_{11\text{cis},m} = 0 \quad (4a)$$

$$c_{13\text{cis},i} - a_{nm}\Delta c_{13\text{cis},n} - b_{nm}\Delta c_{13\text{cis},m} = 0 \quad (4b)$$

For $S_{13\text{cis},nm}$:

$$c_{11\text{cis},i} - a_{nm}\Delta c_{11\text{cis},n} - b_{nm}\Delta c_{11\text{cis},m} = 0 \quad (4c)$$

$$c_{\text{AT},i} - a_{nm}\Delta c_{\text{AT},n} - b_{nm}\Delta c_{\text{AT},m} = 0 \quad (4d)$$

For $S_{11\text{cis},nm}$:

$$c_{\text{AT},i} - a_{nm}\Delta c_{\text{AT},n} - b_{nm}\Delta c_{\text{AT},m} = 0 \quad (4e)$$

$$c_{13\text{cis},i} - a_{nm}\Delta c_{13\text{cis},n} - b_{nm}\Delta c_{13\text{cis},m} = 0 \quad (4f)$$

It should be noted that the conditions for a_{nm} and b_{nm} (eqs 4a–4f) imposed on eq 3, together with the normalization of the concentrations, described in the previous section, lead to $c_{\text{AT},i} - a_{nm}\Delta c_{\text{AT},n} - b_{nm}\Delta c_{\text{AT},m} = 1$ (see the Appendix), a factor which therefore can be omitted in eq 3.

The error in the obtained spectra is mainly caused by the inaccuracy of the difference spectra, especially for large coefficients a_{nm} and b_{nm} . Therefore, the sets of equations were solved for all combinations of $n, m \in [1, 7]$ and $n \neq m$. In the case of high proximity of all the concentration values of the difference spectra (i.e., $\Delta c_n \approx \Delta c_m$ for all-trans, 13-cis, and 11-cis retinal), the magnitudes of the coefficients a_{nm} and b_{nm} are very high, leading to a large uncertainty of the obtained spectrum. Hence, the spectrum was only accepted for $|a_{nm}|, |b_{nm}| < 8$ for $S_{\text{AT},nm}$ and $S_{13\text{cis},nm}$ and $|a_{nm}|, |b_{nm}| < 7.5$ for $S_{11\text{cis},nm}$ (resulting in an average of 10, 12, and 13 spectra in the case of S_{AT} , $S_{13\text{cis}}$, or $S_{11\text{cis}}$). The resulting spectra showed a comparable and low signal-to-noise ratio and a high degree of similarity, especially in the case of $S_{11\text{cis}}$. The error associated with each spectrum could be assumed to have resulted mostly from the poor assumption of the presence of only three species in the sample. The peak characteristics (see Table 2) were calculated as the weighted mean of the characteristics of each spectrum. Due to the high similarity of error in all the obtained spectra and their comparable low magnitude, this mean was in practice the

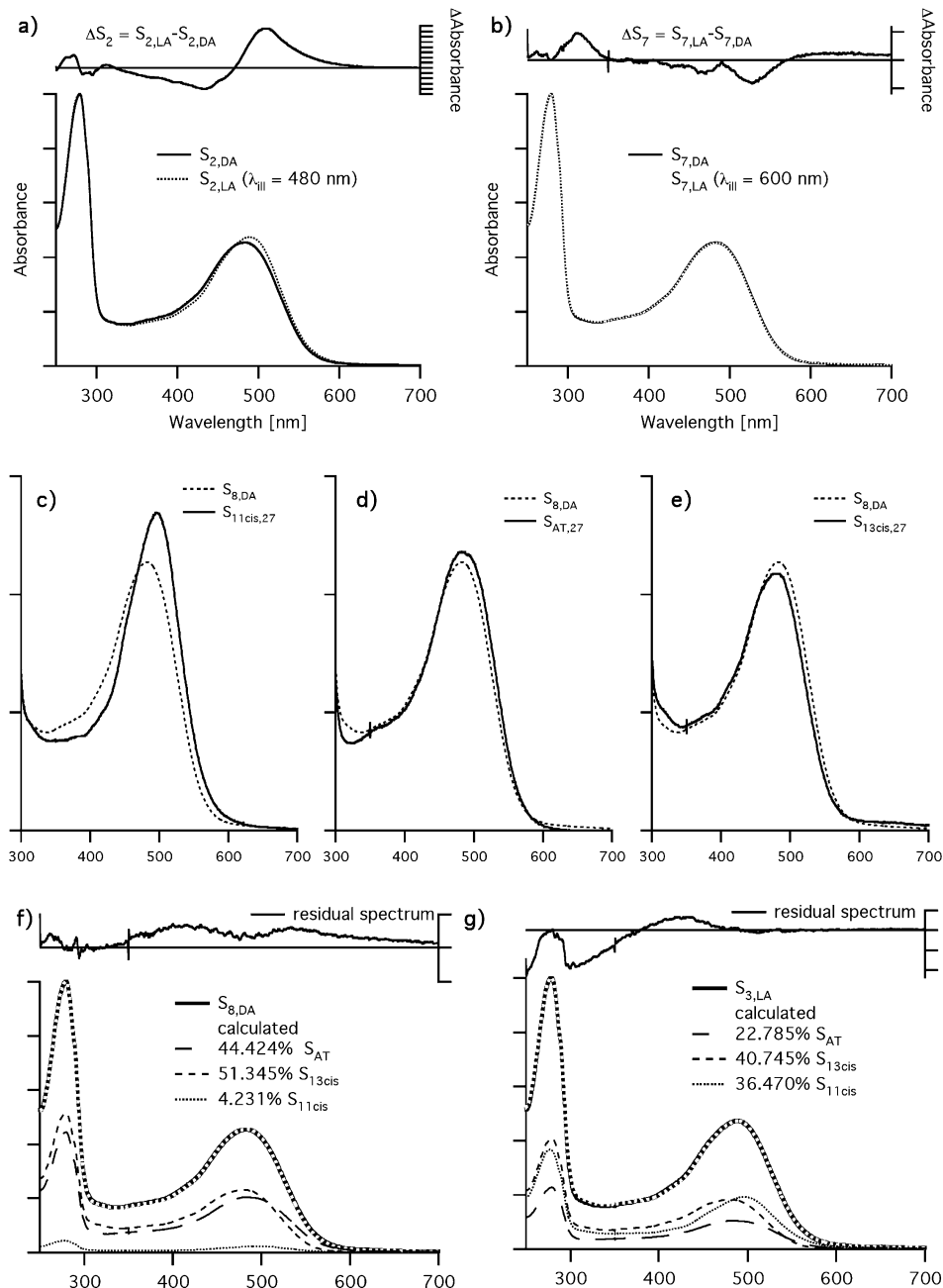


Figure 2. Sketch of the extraction of the single component UV-vis spectra $S_{11\text{cis}}$, S_{AT} , and $S_{13\text{cis}}$. To obtain the single component spectra $S_{11\text{cis},27}$ (c), $S_{\text{AT},27}$ (d), and $S_{13\text{cis},27}$ (e), the difference spectra ΔS_2 (a) and ΔS_7 (b) were subtracted from the dark adapted spectrum $S_{8,DA}$ using eq 3, with the coefficient $a_{11\text{cis}} = 3.118$ and $b_{11\text{cis}} = -2.125$, $a_{\text{AT}} = 0.598$, and $b_{\text{AT}} = -6.753$ and $a_{13\text{cis}} = -0.774$ and $b_{13\text{cis}} = 6.018$, respectively. The spectra $S_{11\text{cis}}$, S_{AT} , and $S_{13\text{cis}}$ were calculated as an average of all single component spectra obtained by using different difference spectra with selection criteria of $|a|, |b| < 8$ for $S_{\text{AT},\text{nm}}$ and $S_{13\text{cis},\text{nm}}$ and $|a|, |b| < 7.5$ for $S_{11\text{cis},\text{nm}}$ (resulting in an average of 10, 12, and 13 spectra in the case of S_{AT} , $S_{13\text{cis}}$, or $S_{11\text{cis}}$). Using the obtained single component spectra, all the measured spectra could be reproduced to a very high precision (e.g., f, g). One division of the left and right y-axis corresponds to 0.2 and 0.005 absorbance units, respectively.

simple mean, and also the error was reduced to the square root of the variance. The peak characteristics showed all an error of less than 5%. Therefore, as a first approximation, the average spectra were calculated as a simple average of all accepted spectra. The slight uncertainty of the height of the peak around 500 nm is mainly caused by the fact that the only difference spectrum showing a positive change in 13-cis retinal, and a very low change in all-trans retinal, is ΔS_7 (see Figure 2b), while all the other single component spectra had to be obtained from

the subtraction of difference spectra which followed the same trend.

The reliability of the obtained single component spectra S_{AT} , $S_{13\text{cis}}$, or $S_{11\text{cis}}$ was tested by reproducing all 16 experimentally obtained spectra (e.g., Figure 2f,g). The reproduced spectra showed high agreement with the experimental spectra. The calculated residual spectra are characterized by broad spectral features of comparably low magnitude, which can be explained by the assumption made at the beginning that only three species were present in the samples. However, these features

Table 2. Obtained Peak Characteristics of the Absorbance Peak around 500 nm for the MR Proteins Binding 13-cis, All-trans, and 11-cis Retinal^a

retinal	λ_{max} (nm)	Abs _{max} normalized	fwhm (nm)
13-cis	479 ± 2	0.45 ± 0.02	122 ± 5
all-trans	485 ± 2	0.46 ± 0.02	123 ± 5
11-cis	495 ± 1	0.53 ± 0.02	99 ± 5

^aThe values are obtained from Figure 3, and the errors are estimated from the variance of the characteristics of all the absorption spectra used for calculating the average spectra.

are comparably small and have a small influence on the peak characteristics, which supports the reliability of the chosen method for the calculation of S_0 and the obtained spectra.

Time-Resolved Flash Photolysis Study in the Microsecond Time Region. Time-resolved flash photolysis, with various excitation wavelengths, was used to study the transient absorption change of MR in the microsecond time region. The flash photolysis setup for this purpose enabled the study of the red-shifted intermediates as well as the bleaching of the original state in high time resolution. In this setup, the output of a wavelength tunable dye laser (FL3002, Lambda Physik, Göttingen, Germany) pumped by a XeCl excimer laser (LEXTRA 50, Lambda Physik, Göttingen, Germany) was used as an excitation light. The sample solution was placed in a quartz cuvette (path length = 2 mm, O.D. = 2.5). The used excitation wavelengths were 454, 485, and 520 nm corresponding to the shorter, middle, and longer wavelength parts of the initial state MR absorption. The repetition rate and power of the laser were 5 Hz and 1 mJ/pulse, respectively. The transmitted probe light from a Xe lamp (L9289-01, Hamamatsu Photonics K. K., Hamamatsu, Japan) was monochromated by a monochromator, and the intensities were measured by a photomultiplier tube (R10699, Hamamatsu Photonics K. K., Hamamatsu, Japan) at 490 and 570 nm. The transient absorption changes were obtained by calculating the ratios between the intensities of the transmitted light before and after sample excitation. 500 traces were averaged to improve the signal-to-noise ratio, and the obtained data was stored in a computer.

Flash Photolysis Study in the Submillisecond to Subsecond Time Region. A second flash photolysis setup (of lower time resolution) was used to study the formation and decay of slower intermediates over the entire spectral range, including blue-shifted intermediates such as the M-intermediate, to obtain a complete 2-D plot of the changes in absorption after photoillumination. For that purpose, an ICCD linear detector (Photonic Multichannel Spectral Analyzer PMA-11 C8808-01, Hamamatsu Photonics K. K., Hamamatsu, Japan) was used which has a high sensitivity for the near-UV to visible light (which includes the region where the M absorption is expected to be observed). The sample solution was placed in a quartz cuvette (path length = 10 mm, O.D. = 0.5), and was illuminated with a beam from an OPO system (LT-2214, LOTIS TII, Minsk, Republic of Belarus) excited by the third harmonics of a nanosecond pulsed Nd³⁺-YAG laser (λ = 355 nm, LS-2134UTF, LOTIS TII, Minsk, Republic of Belarus). The repetition rate and power of the laser were 5 Hz and 300 μ J/pulse, respectively. The intensities of the transmitted probe light from a Xe lamp (L8004, Hamamatsu Photonics K. K., Hamamatsu, Japan) were measured before and after sample excitation, and the transient absorption spectra were obtained

by calculating the ratio between them. The delay time of the spectrum acquisition after excitation was increased from 80 to 180 ms in equal intervals on a logarithmic time scale. The total number of acquired time points was 83. 100 spectra were averaged to improve the signal-to-noise ratio at each time point, and the obtained data was stored in a computer. To obtain the time-evolution profiles of the changes in absorbance at specific probe wavelengths, the time traces of the signals included in the specific probe wavelength regions of a 10 nm width were averaged.

RESULTS

Retinal Composition under Varying Light Conditions as Revealed by HPLC Analysis. A sample of MR consists, in general, of proteins binding all-trans, 13-cis, and 11-cis retinal, with relative compositions depending on external sample conditions. The composition of eight samples of MR were studied, which were illuminated with a particular light of a range of wavelengths λ_{ill} (see Table 1). Table 1 also shows the normalized values of the HPLC analysis of those samples after adaptation for several days in the dark and under illumination. As can be seen, in the dark, the main retinal conformations found are 13-cis (~50%) and all-trans (~44%). Upon illumination with light of $\lambda_{\text{ill}} = 450$ nm, the composition changes dramatically, showing a sharp increase in the presence of the 11-cis retinal isomers (+33%) and a decrease in the concentration of all-trans (-20%) and 13-cis (-13%) retinal. When increasing the illumination wavelength λ_{ill} , the changes in the all-trans retinal composition first increase slightly, reaching a maximum of about -24% at $\lambda_{\text{ill}} = 550$ nm, after which the all-trans concentration stays more stable, while the number of proteins binding 13-cis retinal shows a constant decline in its negative concentration change, decreasing down to $\lambda_{\text{ill}} = 600$ nm, when the 13-cis retinal concentration even increases (+6.5%). The decreases in all-trans and 13-cis retinal are counterbalanced by an increase in 11-cis retinal, which is strongest at short wavelengths, while, for wavelengths of $\lambda_{\text{ill}} \geq 600$ nm, almost no change in 11-cis retinal composition has been observed. One should also have in mind that, upon illumination, a trace amount of other retinal conformations appears.

Absorption Properties of Each Chromophore. To compare the absorption properties of MR binding all-trans, 13-cis, or 11-cis retinal, the pure absorption spectra of each component have to be obtained. However, in conditions known so far, it is not possible to obtain a sample containing predominantly one retinal form, and therefore, the optical information of a pure sample has to be extracted from the absorption spectra of samples having a mixture of retinal conformations. Using the analysis introduced above, we succeeded in extracting the single component spectra of all-trans retinal S_{AT} , 13-cis retinal $S_{13\text{cis}}$, and 11-cis retinal $S_{11\text{cis}}$ (see Figures 2 and 3). The high quality of the obtained spectra allowed us to reproduce all experimentally obtained mixed MR spectra (see, e.g., Figure 2f and g). It is worth mentioning that previously also another strategy was reported for obtaining pure absorption spectra.¹⁶ This method obtains the spectra from bleached rhodopsin which was regenerated with a pure retinal isomer. The comparison of the spectra obtained with both methods could be used to study how such a regenerated protein differs from its original state, a problem which could be omitted in our method. Thus, the spectra can be used for the comparison of the positions and relative heights of the

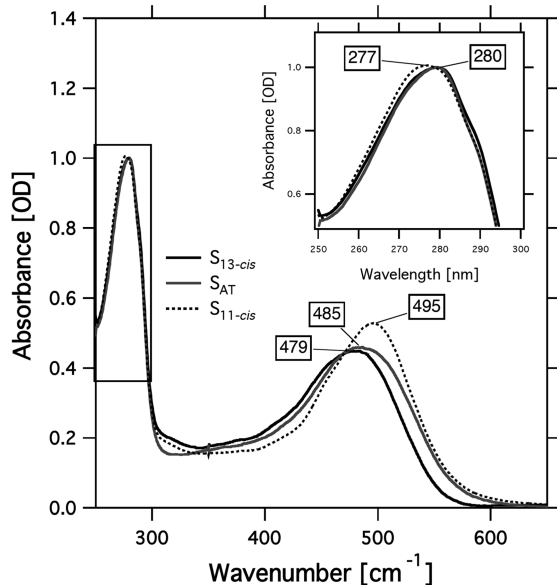


Figure 3. Single component absorption spectra of all-*trans*, 13-*cis*, and 11-*cis* retinal obtained after solving eq 3 for all difference spectra obtained, and averaging the obtained results (see also Figure 2).

absorption peaks (see Table 2). The maximum of the peak, corresponding to the chromophore and its environment, is located around 479 nm in the case of a sample containing only 13-*cis* retinal, and red-shifted by 6 or 16 nm in the case of 100% all-*trans* retinal (485 nm) or 11-*cis* retinal (495 nm), respectively (see Figure 3). Furthermore, simultaneously to the occurring shift, the molecular extinction coefficient of the protein increases, especially in the case of proteins binding 11-*cis* retinal, the spectra of which also shows a comparably narrow peak. It should also be noted that the formation of the 11-*cis* retinal isomer induces a slight blue-shift of the second observed peak from 280 to 277 nm, corresponding to certain Trp and/or Tyr residue(s) (see inset in Figure 3).

Photoreaction Dynamics of MR. In a next step, flash photolysis measurements were conducted to study the photoreaction dynamics of MR binding all-*trans*, 13-*cis*, or 11-*cis* retinal. To obtain the time traces of the changes in absorption in the micro- and subsecond time domains, measurements with two types of experimental setups were performed. For the fast microsecond time region, a photomultiplier tube was used to detect the intensity of the transmitted probe light, while for the slower time region (submillisecond to subsecond) an ICCD camera was used to obtain the difference absorption spectra at successive time points. Furthermore, the difference absorption spectra were also measured at a small number of time points in the microsecond time region by the ICCD camera to observe the changes in the whole spectral range. These measurements enabled us to obtain complete 2-D (wavelength vs time) plots of the changes in absorption after the photoillumination.

Figure 4a shows the transient absorption spectra in the microsecond time region after illumination with three different excitation wavelengths (454, 485, and 520 nm) to activate those MR proteins binding preferentially all-*trans*, 13-*cis*, or 11-*cis* retinal in the sample. For all used excitation wavelengths, a bleaching of MR was observed around 490 nm, while around 570 nm the accumulation of a red-shifted product species could be followed. Interestingly, the absorption maxima of the red-

shifted intermediates were more red-shifted with increasing excitation wavelength from 556 nm (454 nm excitation) to 578 nm (520 nm excitation) (Figure 4a). The time evolution of the absorption changes were recorded at high time resolution at two different probe wavelengths (490 and 570 nm) to monitor mainly the bleaching of MR or the accumulation of a red-shifted intermediate (Figure S1, Supporting Information). All traces shown in Figure S1 could be reproduced by the sum of two exponential functions and a constant value. This constant value indicates that a part of the invoked change in absorption remains even after 100 ms. The obtained lifetimes were independent of the excitation wavelength used, and could therefore be averaged, while their relative intensities differed, suggesting that all photoreactions originating from all three isomers were initiated at all excitation wavelengths, but the relative extent of them depended on the wavelengths of the excitation light. This is expected given the close absorption properties of the MR proteins binding all-*trans*, 13-*cis*, or 11-*cis* retinal (see Figure 3). The averaged lifetimes τ_1 and τ_2 of the exponents used for the fitting of the traces in Figure S1 in the Supporting Information are similar for both probe wavelengths, and could be, therefore, summarized as representing the same event (see Table 3). The errors indicate how strong the event corresponding to either τ_1 or τ_2 was observed at the corresponding probe wavelength. In the further analysis of those events, the values of higher precision were used to represent the lifetimes of the events.

The transient absorption spectra in the slower millisecond time region are shown in Figure 4b. The temporal changes in absorbance along specific probe wavelengths were extracted by accumulating the signal around this wavelength in a 10 nm width; i.e., for monitoring mainly the red-shifted intermediate, the bleaching of the initial state or the blue-shifted intermediate, the intervals were chosen to be 560–570, 490–500, and 394–404 nm, respectively [see Figure 5 (thin solid lines)]. The time dependencies of these traces were relatively complex compared to the evolution of the traces obtained in the faster time region (Figure S1, Supporting Information) caused by the spectral overlap of those events. Thus, 2, 3, and 4 exponential functions were required to reproduce the traces representing mainly the accumulations of the blue- and red-shifted intermediates and of the bleaching of MR, respectively. Also in this case, the relative intensities of the exponential functions were dependent on excitation wavelength, while the lifetimes of all exponential components did not change. Therefore, the corresponding lifetimes obtained by the measurements with different excitation wavelengths could as well be averaged. Furthermore, it should be noted that also in this time regime some of the averaged lifetimes obtained at different probe wavelengths were similar, within experimental error, which indicates that they represent the same reaction processes. On the basis of this consideration, all obtained lifetimes in the slower time region were categorized and summarized (see Table 4).

As can be seen in Table 4, four reaction steps in the submillisecond to subsecond time domain could be identified. Furthermore, when comparing the results to the ones obtained in the faster time region shown in Table 3, it can be noted that τ_2 and τ_3 are in the same order of magnitude, which indicates that they could be assigned to the same reaction step (the slightly larger value for τ_3 might be caused by the low time resolution of the ICCD used for this measurement). Furthermore, this is in accordance with the similarity of their dependence on excitation wave-

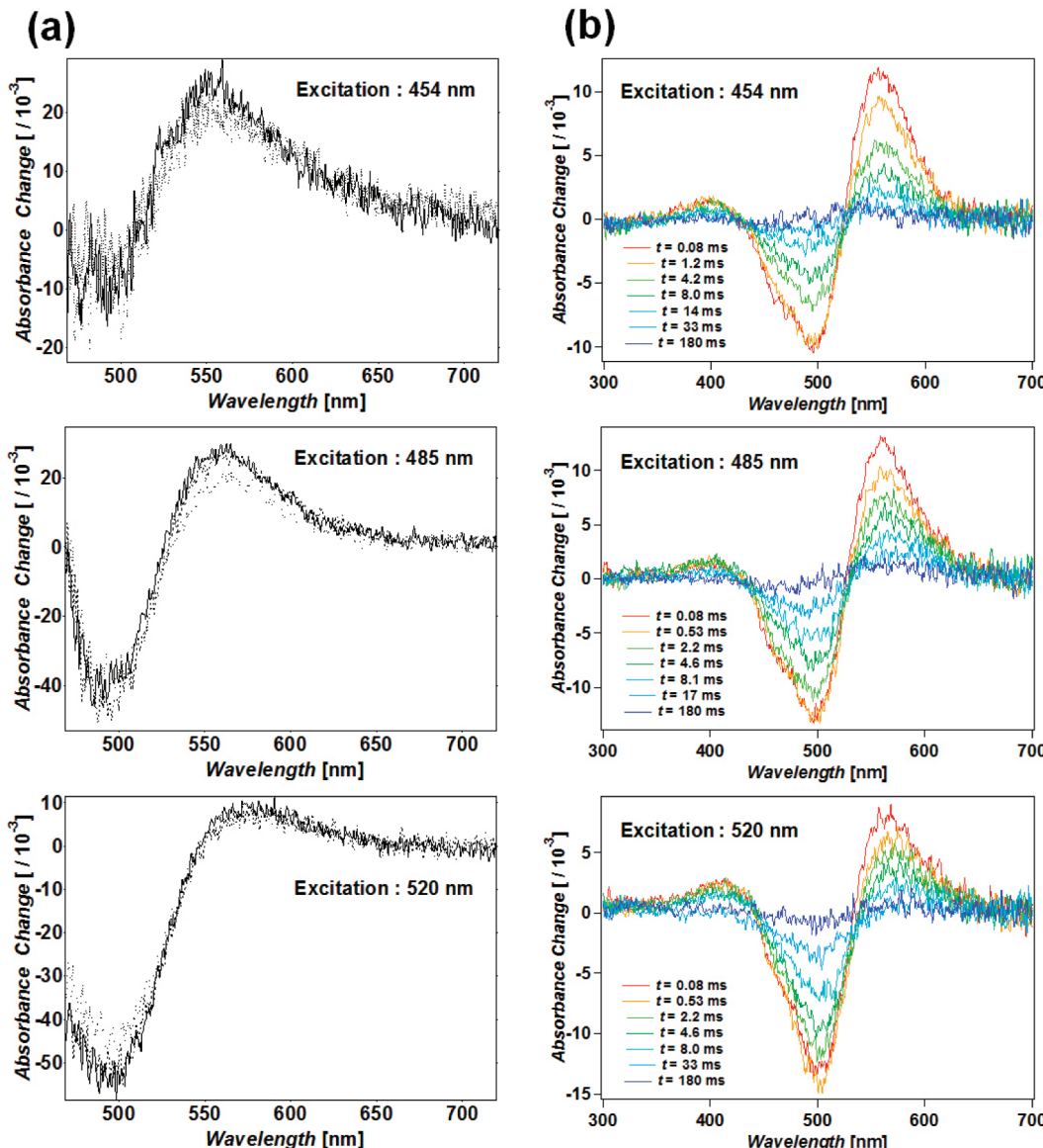


Figure 4. (a) Transient absorption spectra of MR at three different excitation wavelengths (454, 485, and 520 nm) in the microsecond time region. The delay times were 1 (solid line), 5 (dashed line), and 100 μ s (dotted line). (b) Transient absorption spectra of MR at three different excitation wavelengths (454, 485, and 520 nm) in the submicro- to millisecond time region.

Table 3. Averaged Lifetimes τ_1 and τ_2 of the Exponential Components Identified by the Fitting of the Absorption Change with Time at Each Probe Wavelength in Figure S1 (Supporting Information)^a

probe wavelength (nm)	τ_1 (μ s)	τ_2 (μ s)
490	14 ± 12	93 ± 12
570	8.2 ± 1.5	70 ± 30

^aThe values in bold were chosen to represent the lifetimes of the corresponding event due to stronger occurrence in the corresponding time trace.

length. Therefore, the remaining five components (τ_1 , τ_2 , τ_4 – τ_6) can be considered to represent the actual reaction processes of MR.

Putative Assignment of the Lifetimes to Their Reaction Processes. As already mentioned, an MR sample is represented by a mixture of proteins binding all-*trans*, 13-*cis*, or 11-*cis* retinal. In this study, five reaction components (τ_1 , τ_2 ,

τ_4 , τ_5 , τ_6) at intensities depending on the excitation wavelength of the sample were obtained which correspond to the photoreactions of the proteins in the sample. On the basis of the general knowledge of microbial rhodopsins, as well as the absorption properties (see Figure 3), we propose a way of assigning those lifetimes to photointermediates in a possible photocycle.

First, the intermediates in the blue probe wavelength region (394–404 nm) will be considered. The main change in absorption in this region decays with τ_5 . It is evident from the literature on microbial rhodopsins that transient species showing an absorption in this region have, in general, a deprotonated retinal Schiff base, like, e.g., the M-intermediate of BR.^{17,18} Furthermore, all of the reported blue-shifted intermediates are generated by the excitation of an all-*trans* isomer (for example, while the all-*trans* form of BR generates an M-intermediate, the 13-*cis* isomer does not). Therefore, it can be assumed that also here the decay of an M-intermediate

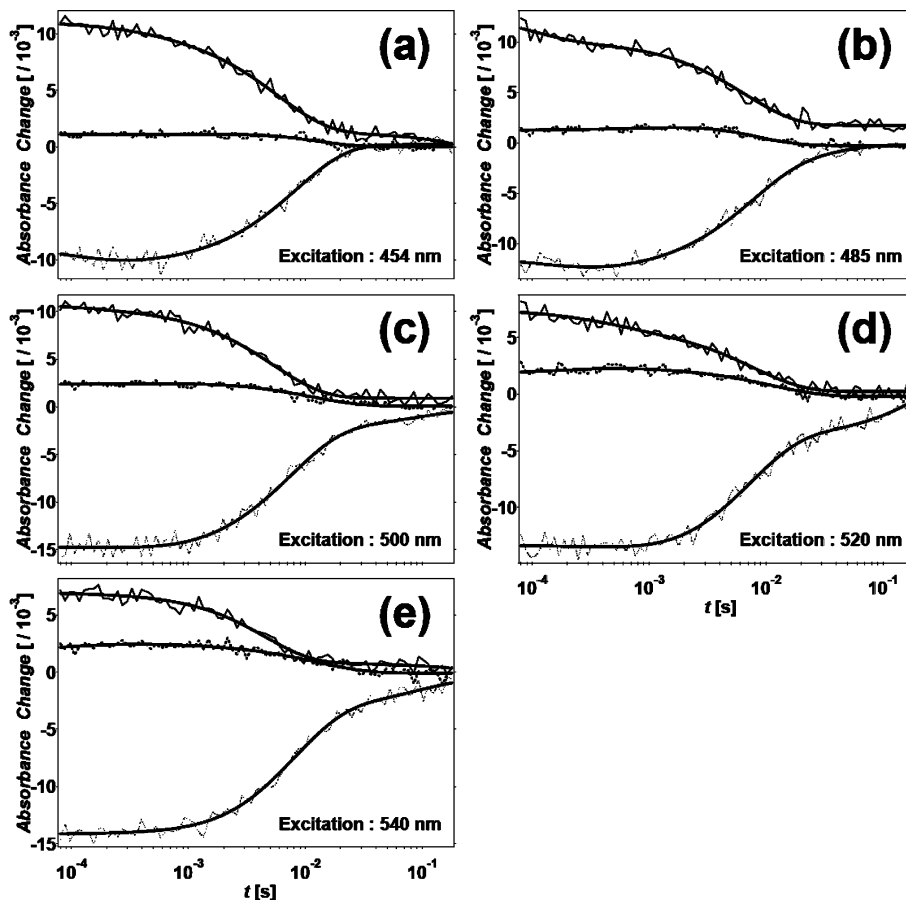


Figure 5. Transient absorption change of MR in the submilli- to subsecond time region (the delay time was between 80 μ s and 180 ms) at five excitation wavelengths: (a) 454, (b) 485, (c) 500, (d) 520, and (e) 540 nm. To observe the temporal evolution of the bleaching of the initial state (dotted line), the signals between 490 and 500 nm were averaged to improve the signal-to-noise ratio. Similarly, the temporal evolution of the accumulations of blue- and red-shifted intermediates (dashed and thin solid lines) was obtained by averaging the signal of the probe wavelengths from 394 to 404 nm and 560 to 570 nm, respectively. The bold solid lines represent the best fits using 2, 3, or 4 exponential components.

Table 4. Averaged and Categorized Lifetimes τ_3 – τ_6 of the Exponential Components Identified by the Fitting of the Absorption Change with Time in Each Probe Wavelength Interval in Figure 5^a

probe wavelength (nm)	τ_3 (ms)	τ_4 (ms)	τ_5 (ms)	τ_6 (ms)
394–404	0.14 ± 0.05	N.O.	12.0 ± 0.4	N.O.
490–500	0.49 ± 0.14	5.3 ± 1.1	14 ± 5	179 ± 34
560–570	0.094 ± 0.016	5.1 ± 1.1	N.O.	273 ± 50

^aN.O.: not observed. The values in bold were chosen to represent the lifetimes of the corresponding event due to stronger occurrence in the corresponding time trace. τ_3 is considered to represent the same reaction process as τ_2 (see text).

generated from the excited all-*trans* form of MR is observed. To reinforce this assignment, the excitation wavelength dependence of the amplitude of this component is considered (Figure 6), and compared to the pure absorption spectrum of the all-*trans* isomer (see Figure 3). The amplitude of the M-decay component showed a maximum at around 500 nm (Figure 6) which is close to the λ_{max} of the all-*trans* isomer (485 nm) (Figure 3). The small difference of wavelength might be caused by the occurrence of multiple M-like blue-shifted intermediates, as are found in BR, SRI, and SRII^{19–21} and/or by the adaptation pathway from/to the all-*trans*, 13-*cis*, and 11-*cis*

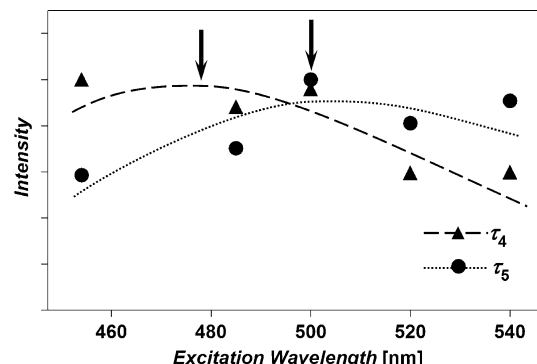


Figure 6. Relative amplitudes of the fitting components of (▲) τ_4 at the 560–570 nm probe wavelength interval and of (●) τ_5 at the 394–404 nm interval (see Figure 5), depending on excitation wavelength. The dashed and dotted lines are drawn arbitrary to indicate the putative peak positions of the data points.

forms. On the basis of these facts, τ_5 was assigned to the M decay formed by the excitation of the all-*trans* isomer.

Next, the component with the lifetime τ_4 in the trace of the red-shifted absorption change (thin solid line in Figure 5) will be considered. It should be noted that also the signal associated with the bleaching of MR (dotted lines in Figure 5) has this component as a rising signal. Therefore, τ_4 represents the

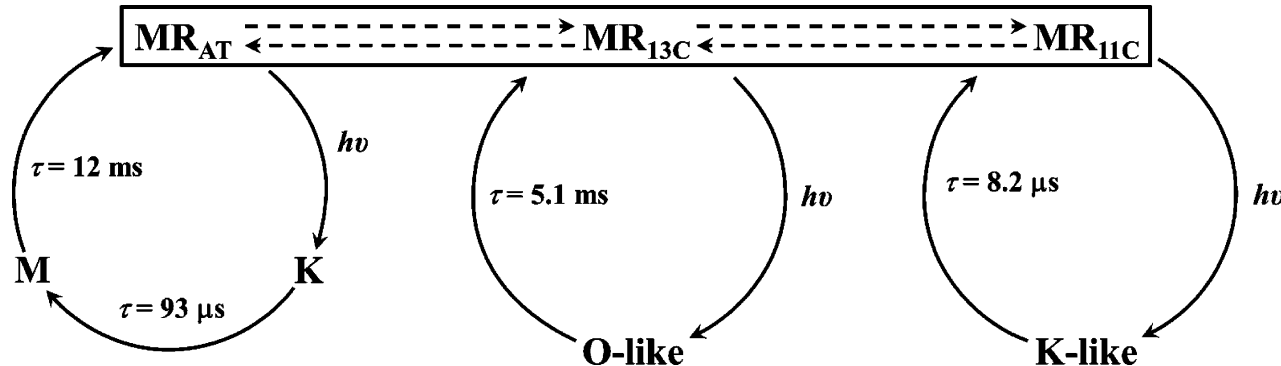


Figure 7. Schematic illustration of the photocycles of MR, determined by the flash photolysis measurements. In the dark state, MR proteins binding all-trans, 13-cis, and 11-cis retinal exist in equilibrium. After light excitation, the all-trans retinal form is converted to a K-intermediate, followed by an M-intermediate. Both proteins binding 13-cis and 11-cis retinal show only a red-shifted intermediate (O- and K-like, respectively).

recovery from a red-shifted species to the initial state. Also the intensity of this component is dependent on excitation wavelength (see Figure 6). In contrast to the signal attributed to the M decay (τ_3), the amplitude of this component becomes stronger with relatively shorter excitation wavelengths (454–500 nm). This distribution is similar to the pure absorption spectrum of the 13-cis isomer (Figure 3). In addition, it has been reported that the photoexcited 13-cis isomer of BR in a dark state produces an O-like red-shifted intermediate which recovers directly to the original state with a lifetime of tens of milliseconds²² similar to that of τ_4 (5.1 ms). These considerations support the assignment of τ_4 to the decay of an O-like intermediate generated by the excitation of the 13-cis form. This O-intermediate is likely to directly decay to the initial state, and to therefore close the photocycle of this isomer.

In the faster time region, two decaying components (τ_1 and τ_2) were observed, both in the signal of the red-shifted probe wavelength. Those components can be assumed to be linked to the decay of an intermediate of the 11-cis isomer, as well as a K-intermediate in the photocycle of the protein binding all-trans retinal. The presence of a K-intermediate in the photocycle is expected because it always precedes the formation of the M-intermediate in microbial rhodopsins reported in the literature. The formation of the M-intermediate was observed in Figure 5 as a rising component at the 394–404 probe wavelength with the lifetime τ_3 . Because τ_3 was considered to represent the same reaction step as τ_2 , the red-shifted intermediate with the lifetime τ_2 can be assumed to correspond to the K-intermediate formed by the excitation of the all-trans isoform, after which it converts to the M-intermediate. In addition, we recently observed the decay process of a K-intermediate from the all-trans form by step-scan Fourier-transform infrared (FTIR) spectroscopy with lifetimes of 73.3 μ s (major component, 87%) and 356 μ s (minor component, 13%) being similar to τ_2 obtained in the present study (Furutani et al., unpublished data). Thus, the result obtained by this step-scan FTIR spectroscopy study is consistent with the current assignment. Finally, it is likely that the τ_1 component can be considered to be associated with the 11-cis isomer (Figure 3). However, the error of the amplitude of this component is too high to enable a sufficient comparison with the absorption spectrum of the 11-cis isoform. This comparably large error is probably caused by the insufficient S/N ratio of our measurement system in the $\tau < 10 \mu$ s time region.

In a next step, the slowest decaying component (τ_6) remains to be assigned. However, due to the very small amplitudes, and its highly complicated excitation wavelength, it cannot be assigned to any reaction process of MR with certainty (although its assignment to the decay of an O-intermediate generated after the M-intermediate of the all-trans form is likely).

Finally, the results from this analysis of the signal assignment have been schematically summarized in Figure 7.

■ DISCUSSION

MR has been identified as a member of the microbial rhodopsin family, located, evolutionarily, at the middle position between BR and SRII. However, the composition of its retinal chromophore is very unusual, containing three retinal isomers: all-trans, 13-cis, and 11-cis. So far, only a type-2 rhodopsin, retinochrome, was reported to bind 11-cis retinal, and its photoexcitation triggers an isomerization to all-trans.³ In this process, the all-trans retinal is released to the environment, while MR shows a cyclic photoreaction. Thus, the photoreaction process of MR is highly complex and unique, compared with other type-1 or type-2 rhodopsins. This complexity motivated us to conduct a complex flash photolysis study, combined with the study of the excitation wavelength dependency of the absorption spectra of each isomer, and the composition of the retinal isomers in light-adapted states.

Absolute Absorption Spectra of MR. The retinal composition in the light-adapted state showed a high dependence on the excitation wavelength (Table 1). While the all-trans and 13-cis forms were abundant at longer wavelengths ($\lambda_{\text{ill}} > 600 \text{ nm}$), the 13-cis and 11-cis forms became dominant at shorter wavelengths ($\lambda_{\text{ill}} < 580 \text{ nm}$). Furthermore, the absolute absorption spectra of these isomers (Figure 3) showed their λ_{max} to be shifted in the order of 13-cis (479 nm) < all-trans (485 nm) < 11-cis (495 nm) retinal, with the extinction coefficient of the 11-cis form being significantly larger than those of the other isomers. The λ_{max} of all isomers are much shorter than that of BR (560 nm), and similar to that of SRII (498 nm). This implies that the blue-shift of the λ_{max} in the molecular evolution from BR to SRII was already almost completed in MR. However, the λ_{max} of all-trans MR (486 nm) is slightly shorter than that of SRII, and the characteristic spectral shoulder of SRII is not observed in the spectrum of MR. According to the interpretation of fine structures by Takahashi et al.,²³ this indicates that the retinal molecule is not restricted. In general, the λ_{max} corresponds to the most probable

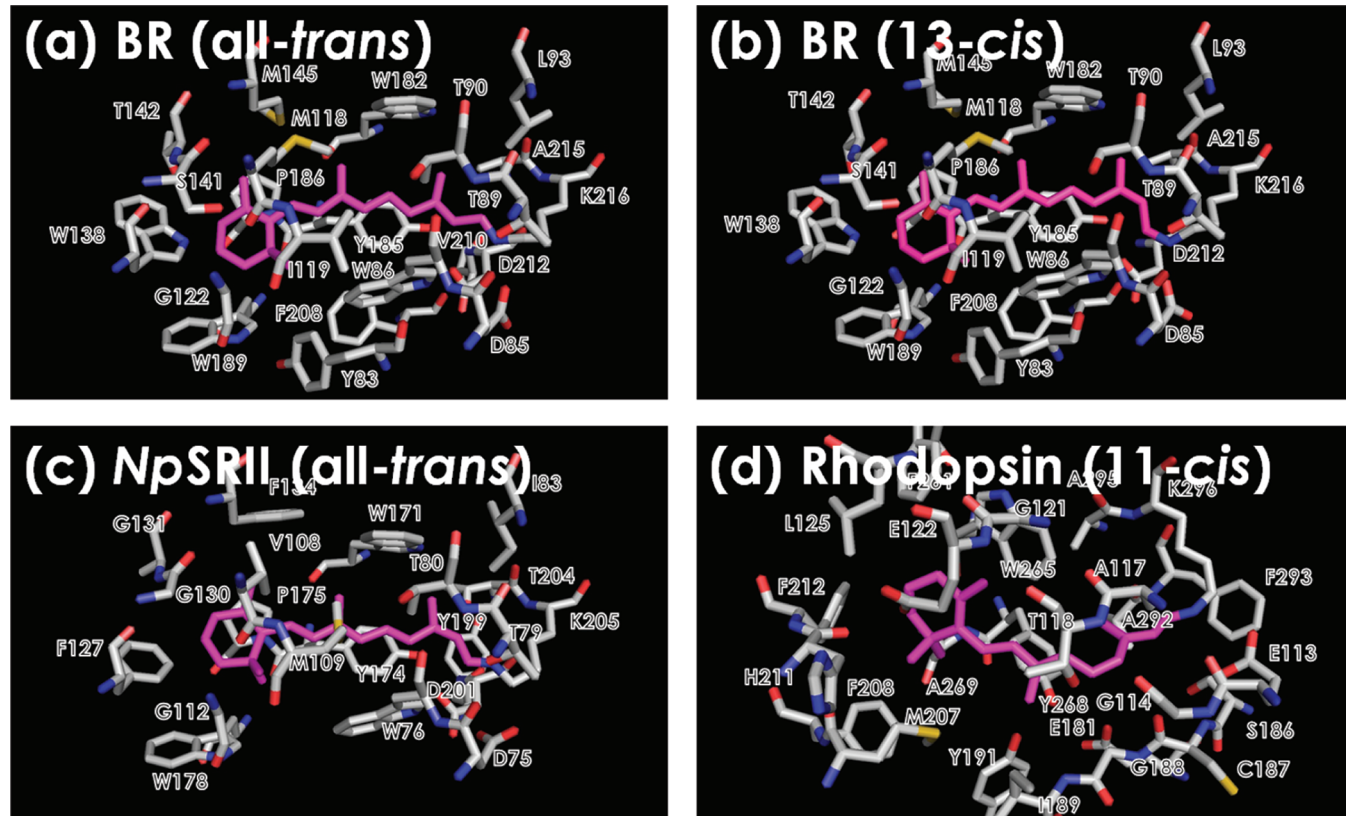


Figure 8. Structure of the retinal binding pockets of (a) BR in the all-trans form (PDB code: 1KGB), (b) BR in the 13-cis form (PDB code: 1X0S), (c) NpSRII (PDB code: 1GUE), and (d) bovine rhodopsin (PDB code: 1U19) based on X-ray crystallographic structures. The amino acids located within 5 Å of the retinal are depicted with their sequence numbers.

transition from the ground to the excited state, and it is well-known that an increase in the 13-cis retinal isomer causes a spectral blue-shift in microbial rhodopsins, which is also observed in MR. Furthermore, the observed red-shift of the 11-cis isomer could be explained by several mechanisms: (i) the weak electrostatic interaction between the protonated Schiff base and its counterion or hydrogen bond acceptor; (ii) an alteration in the polarity or polarizability of the environment of the chromophore-binding site, caused by the arrangement of polar or aromatic residues; and (iii) a planarization around the 6-S bond (6,7-torsion angle) connecting the polyene chain to the β -ionone ring (see Figure 1). Although, the lack of structural information of MR makes it hard to support one of these mechanisms, one should note that the formation of the 11-cis retinal form induces also a slight blue-shift of the peak corresponding to certain amino acids like Trp, Tyr, and/or Phe, from 280 to 277 nm (see inset of Figure 3). Therefore, the mechanism described in argument ii could, among other things, be expected to cause the spectral red-shift of the 11-cis isomer of MR. Furthermore, as shown in Table 2, the half width of the MR binding 11-cis retinal is significantly smaller than those of the 13-cis and all-trans isomers. These results suggest some structural differences between MR with 11-cis retinal and MR binding the all-trans (13-cis) form, and that the structural fluctuations and heterogeneity of the 11-cis isomer of MR are smaller than those of the other isomers. This could be explained by a volume change between the all-trans isomer and the 13-cis or 11-cis retinal form. Figure 8 shows the crystal structures of all-trans BR, 13-cis BR, and all-trans SRII. The retinal chromophores are tightly packed within conserved

aromatic residues, such as Trp, Tyr, and Phe. In the case of an isomerization from all-trans to 13-cis retinal, a double bond ($C13=C14$) is rotated, and therefore, the change in volume (structural rearrangement) is limited (see Figure 1). On the other hand, in the case of 11-cis retinal, a double bond ($C11=C12$) is altered changing also the orientation of a methyl group, which can be expected to induce a larger volume change (structural rearrangement). This can be seen in the structure of bovine rhodopsin (Figure 8d). However, it should be noted that the $C15=N$ bond is likely to be in the 15-syn configuration, for both the 13-cis- and 11-cis isomers, to partly reduce the steric distortion of the opsin moiety imposed by the trans-to-cis isomerization, and further structural and theoretical studies are planned to investigate these questions in the future.

Photocycle of MR. In this study, the photoreaction of each isomer of MR was investigated by flash photolysis measurements using various excitation wavelengths. To decompose the components appearing in the transient absorption change, the relative intensity of each of them at each excitation wavelength was compared to the absolute absorption spectrum of three types of isomers of MR in the dark condition.

The photocycle of the all-trans form contains a K- and an M-intermediate. The lifetime of the K-intermediate was $93\ \mu s$, which is much slower compared to those of BR ($\tau = 1.0\ \mu s$) or SRII ($\tau = 670\ ns$).^{24,25} On the other hand, the decay of the M-intermediate has a lifetime of 14 ms, which is in between that of BR (0.5 ms) and SRII (240 ms). Thus, the dynamics of the all-trans form of MR seem to be in the middle point of the evolution from BR to SRII. In the cases of BR and SRII, the M-intermediate is one of the key intermediates for their function.

Therefore, the M-intermediate of MR can also be expected to be a functionally important state.

The photocycle of the 13-cis form is much simpler, showing only a red-shifted intermediate (O-like intermediate) with a lifetime of $\tau = 5.1$ ms. This is similar to the photocycle of the 13-cis isomer of BR, which shows also a red-shifted photoproduct ($\lambda_{\text{max}} = 585$ nm) with a lifetime of 52 ms.²²

Also, the 11-cis form of MR shows only a red-shifted intermediate in its photocycle. However, its lifetime is much faster ($\tau = 8.2$ μ s) than the one of the O-like intermediate in the 13-cis photocycle ($\tau = 5.1$ ms), making it more similar to that of a K-intermediate, and thus, it is reasonable to call it a K-like intermediate. Because MR is the first microbial rhodopsin which, under physiological conditions, can bind 11-cis retinal, the comparison with other type-1 rhodopsins is difficult. Previously, only the "acid blue" BR₆₀₅ which can be observed by illumination with far-red light at pH 1–3 was reported to have 11-cis retinal.²⁶ This indicates a similarity between the binding pockets of BR and MR required to accommodate the 11-cis chromophore, and is consistent with the phylogenetic position of MR between BR and SRII. However, because BR does not contain 11-cis retinal at physiological conditions, the binding pocket of MR can be expected to be more optimized for its binding. Furthermore, type-2 rhodopsins which bind only 11-cis retinal present several red- and blue-shifted intermediates in their photoreaction pathway (Photo-, Batho-, BSI-, Lumi-, Meta-I, Meta-II, Meta-III intermediates in the case of bovine rhodopsin²⁷) and thus having much more complex photocycles than the 11-cis isomer of MR. Therefore, although binding the same chromophore, the photoreactions of the 11-cis form of MR and type-2 rhodopsins are considerably different.

In conclusion, in this study, we succeeded in determining the absorption properties of the individual MR isomers, as well as the reaction intermediates contained in the photoreaction pathways starting from all of these isomers. However, it should be mentioned that the excitation wavelength dependency of the dynamics of each MR isomer is slightly different from their absolute absorption spectra (Figures 3 and 6), indicating that an unidentified intermediate(s) might exist during the photocycle, and/or that the light adaptation process might affect the photocycle. Furthermore, if some of the isomers show a complete photocyclic reaction, the composition of this isomer(s) should not change in the light adapted state. Therefore, we expect that the reaction pathway of MR is partially or fully branched (the final product is different from the starting species). However, at this stage, another spectroscopic study would be required to reveal the final product of the photoreaction of MR (for example, by monitoring the light adaptation process, and the way the isomeric compositions change with the amount of introduced photons, the efficiency of the reaction between respective isomers could be determined). In addition, it should be noted that all experiments in the present study were performed on MR solubilized in DDM, which imposes a distinctly different environment to its native membrane. Thus, there is a possibility that the obtained compositions of the retinal isomers and spectroscopic properties are different from MR in its native environment. These spectroscopic and biological issues are our next focus.

APPENDIX

In the derivation of eq 3, the following equation was used:

$$c_{\text{AT},i} - a_{nm}\Delta c_{\text{AT},n} - b_{nm}\Delta c_{\text{AT},m} = 1 \quad (\text{A1})$$

In the following, the mathematical proof of this equation is given.

The normalization of the concentrations of all-trans, 13-cis, and 11-cis retinal gives

$$c_{\text{AT},i} + c_{13\text{cis},i} + c_{11\text{cis},i} = 1 \quad (\text{A2})$$

Similar equations can be found for the difference concentrations, using

$$\Delta c_{\text{AT},n} = c_{\text{AT},j} - c_{\text{AT},k} \quad (\text{A3a})$$

$$\Delta c_{13\text{cis},n} = c_{13\text{cis},j} - c_{13\text{cis},k} \quad (\text{A3b})$$

$$\Delta c_{11\text{cis},n} = c_{11\text{cis},j} - c_{11\text{cis},k} \quad (\text{A3c})$$

with (in analogy to eq A2):

$$c_{\text{AT},j} + c_{13\text{cis},j} + c_{11\text{cis},j} = 1 \quad (\text{A3d})$$

$$c_{\text{AT},k} + c_{13\text{cis},k} + c_{11\text{cis},k} = 1 \quad (\text{A3e})$$

By the addition of eqs A3a, A3b, and A3c and by using eqs A3d and A3e, one obtains

$$\Delta c_{\text{AT},n} + \Delta c_{13\text{cis},n} + \Delta c_{11\text{cis},n} = 0 \quad (\text{A3f})$$

and in analogy for index m :

$$\Delta c_{\text{AT},m} + \Delta c_{13\text{cis},m} + \Delta c_{11\text{cis},m} = 0 \quad (\text{A3g})$$

To proof eq A1, one inserts eqs 4a and 4b into eq A2:

$$\begin{aligned} c_{\text{AT},i} &+ (a_{nm}\Delta c_{13\text{cis},n} + b_{nm}\Delta c_{13\text{cis},m}) \\ &+ (a_{nm}\Delta c_{11\text{cis},n} + b_{nm}\Delta c_{11\text{cis},m}) \\ &= 1 \end{aligned}$$

and after reorganizing:

$$\begin{aligned} c_{\text{AT},i} &+ a_{nm}(\Delta c_{13\text{cis},n} + \Delta c_{11\text{cis},n}) + b_{nm}(\Delta c_{13\text{cis},m} + \Delta c_{11\text{cis},m}) \\ &= 1 \end{aligned} \quad (\text{A4})$$

Using eqs A3e and A3f, eq A4 can be written as

$$c_{\text{AT},i} + a_{nm}(-\Delta c_{\text{AT},n}) + b_{nm}(-\Delta c_{\text{AT},m}) = 1 \quad (\text{A5})$$

which is the same as eq A1.

ASSOCIATED CONTENT

S Supporting Information

The time traces of the time-resolved absorption change of MR with various excitation wavelengths in the microsecond time regions are described. This material is available free of charge via the Internet at <http://pubs.acs.org>.

AUTHOR INFORMATION

Corresponding Author

*Phone: +81-52-789-2993. Fax: +81-52-789-3001. E-mail: z47867a@cc.nagoya-u.ac.jp.

Author Contributions

[†]These authors contributed equally to this work.

Notes

The authors declare no competing financial interest.

■ ACKNOWLEDGMENTS

The present work was financially supported in part by a Grant-in-Aid for Scientific Research (KAKENHI) on Priority Area (Area No. 477). This work was also supported by grants from the Japanese Ministry of Education, Culture, Sports, Science, and Technology to K.I. (22018012) and to Y.S. (22018010, 23687019 and 23657100).

■ REFERENCES

- (1) Spudich, J. L.; Jung, K.-H. *Handbook of Photosensory Receptors*; Wiley-VCH: Weinheim, Germany, 2005.
- (2) McCarren, J.; DeLong, E. F. *Environ. Microbiol.* **2007**, *9*, 846–858.
- (3) Terakita, A. *Genome Biol.* **2005**, *6*, 213.
- (4) Waschuk, S. A.; Bezerra, A. G., Jr.; Shi, L.; Brown, L. S. *Proc. Natl. Acad. Sci. U.S.A.* **2005**, *102*, 6879–6883.
- (5) Lanyi, J. K.; Schobert, B. *J. Mol. Biol.* **2003**, *328*, 439–450.
- (6) Nagel, G.; Ollig, D.; Fuhrmann, M.; Kateriya, S.; Musti, A. M.; Bamberg, E.; Hegemann, P. *Science* **2002**, *296*, 2395–2398.
- (7) Nagel, G.; Szellas, T.; Huhn, W.; Kateriya, S.; Adeishvili, N.; Berthold, P.; Ollig, D.; Hegemann, P.; Bamberg, E. *Proc. Natl. Acad. Sci. U.S.A.* **2003**, *100*, 13940–13945.
- (8) Spudich, J. L. *Trends Microbiol.* **2006**, *14*, 480–487.
- (9) Jung, K.-H.; Trivedi, V. D.; Spudich, J. L. *Mol. Microbiol.* **2003**, *47*, 1513–1522.
- (10) Hofmann, K. P.; Scheerer, P.; Hildebrand, P. W.; Choe, H.-W.; Park, J. P.; Heck, M.; Ernst, O. P. *Trends Biochem. Sci.* **2009**, *34*, 540–552.
- (11) Kawanabe, A.; Furutani, Y.; Jung, K.-H.; Kandori, H. *J. Am. Chem. Soc.* **2007**, *129*, 8644–8649.
- (12) Sudo, Y.; Ihara, K.; Kobayashi, S.; Suzuki, D.; Irieda, H.; Kikukawa, T.; Kandori, H.; Homma, M. *J. Biol. Chem.* **2011**, *286*, 5967–5976.
- (13) Sekharan, S.; Morokuma, K. *J. Am. Chem. Soc.* **2011**, *133*, 19052–19055.
- (14) Henry, E. R.; Hofrichter, J. *Methods Enzymol.* **1992**, *210*, 129–192.
- (15) Hendler, R. W.; Shrager, R. I. *J. Biochem. Biophys. Methods* **1994**, *28*, 1–33.
- (16) Maeda, A.; Iwasa, T.; Yoshizawa, T. *J. Biochem.* **1977**, *82*, 1599–1604.
- (17) Braiman, M. S.; Mogi, T.; Marti, T.; Stern, L. J.; Khorana, H. G.; Rothschild, K. *J. Biochemistry* **1988**, *27*, 8516–8520.
- (18) Luecke, H.; Schobert, B.; Richter, H.-T.; Cartailler, J.-P.; Lanyi, J. K. *Science* **1999**, *286*, 255–260.
- (19) Lórenz-Fonfría, V. A.; Kandori, H. *J. Am. Chem. Soc.* **2009**, *131*, 5891–5901.
- (20) Inoue, K.; Sudo, Y.; Homma, M.; Kandori, H. *J. Phys. Chem. B* **2011**, *112*, 2542–2547.
- (21) Klare, J. P.; Gordeliy, V. I.; Labahn, J.; Büldt, G.; Steinhoff, H.-J.; Engelhard, M. *FEBS Lett.* **2004**, *564*, 219–224.
- (22) Gergely, C.; Ganea, C.; Váró, G. *Biophys. J.* **1994**, *67*, 855–861.
- (23) Takahashi, T.; Yan, B.; Spudich, J. L. *Photochem. Photobiol.* **1992**, *56*, 1119–1128.
- (24) Chizhov, I.; Chernavskii, D. S.; Engelhard, M.; Mueller, K. -H.; Hess, B. *Biophys. J.* **1996**, *71*, 2329–2345.
- (25) Inoue, K.; Sasaki, J.; Morisaki, M.; Tokunaga, F.; Terazima, M. *Biophys. J.* **2004**, *87*, 2587–2597.
- (26) Maeda, A.; Iwasa, T.; Yoshizawa, T. *Biochemistry* **1980**, *19*, 3825–3831.
- (27) Vogel, R.; Siebert, F.; Zhang, X.-Y.; Fan, G.; Sheves, M. *Biochemistry* **2004**, *43*, 9457–9466.